

Optimisation of turnout frog profile geometry using revenue service wheel profiles

Jaeik Lee, Arthur de O. Lima, Marcus S. Dersch & J. Riley Edwards

To cite this article: Jaeik Lee, Arthur de O. Lima, Marcus S. Dersch & J. Riley Edwards (05 Jun 2023): Optimisation of turnout frog profile geometry using revenue service wheel profiles, Vehicle System Dynamics, DOI: [10.1080/00423114.2023.2218948](https://doi.org/10.1080/00423114.2023.2218948)

To link to this article: <https://doi.org/10.1080/00423114.2023.2218948>



Published online: 05 Jun 2023.



Submit your article to this journal [↗](#)



Article views: 153




View related articles [↗](#)



View Crossmark data [↗](#)



Optimisation of turnout frog profile geometry using revenue service wheel profiles

Jaeik Lee , Arthur de O. Lima , Marcus S. Dersch  and J. Riley Edwards 

Rail Transportation and Engineering Center – RailTEC, Department of Civil and Environmental Engineering – CEE, Grainger College of Engineering – GcoE, University of Illinois at Urbana-Champaign – UIUC, Urbana, IL, USA

ABSTRACT

Railroad turnouts are an essential element of the track infrastructure that facilitates the movement of trains between adjacent or diverging tracks. Turnout frogs are subjected to high wheel impact forces due to the inherent need for a discontinuity in their geometry. To develop an optimised frog geometry to minimise wheel impacts, a parametric study was designed and executed that considered three critical design parameters: point (i.e. nose) slope, relative height difference between wing and point, and longitudinal wing slope. Four hundred wheel profiles were extracted from a dataset of one million revenue service wheel profiles based on a wheel classification methodology previously developed. Wheel impact was quantified for each frog geometry case based on wheel transfer distribution and vertical wheel trajectory which were analysed using a developed Python algorithm. A total of 30 unique geometries were evaluated, including the existing standard design geometry for a N.A. heavy point conformal frog. Results demonstrated that each parameter affects different locations along the frog and total impact is most affected by point slope. Lastly, an optimised frog geometry was selected that ensures well-distributed wheel transfer locations preventing the concentration of damage, and results in low total impact at the transfer point.

ARTICLE HISTORY

Received 4 October 2022
Revised 24 April 2023
Accepted 23 May 2023

KEYWORDS

Railroad turnout; geometry optimisation; turnout frog; parametric study; impact quantification

Introduction

Background

Railroad turnouts are widely considered to be one of the most critical infrastructure assets given the complexity of their design when compared to other track components and their function in the safe movement of trains. If they are not functioning properly, they can result in maintenance expenditures and even derailments, causing significant track outages and traffic disruptions [1]. Therefore, ensuring adequate wear and impact resistance of frogs (internationally referred to as ‘crossings’) is crucial, especially in high and higher-speed rail operations and the demanding heavy axle load (HAL) freight railroad operating environment in North America (N.A.). According to the U.S. Department of Transportation

CONTACT Jaeik Lee  jaeik2@illinois.edu

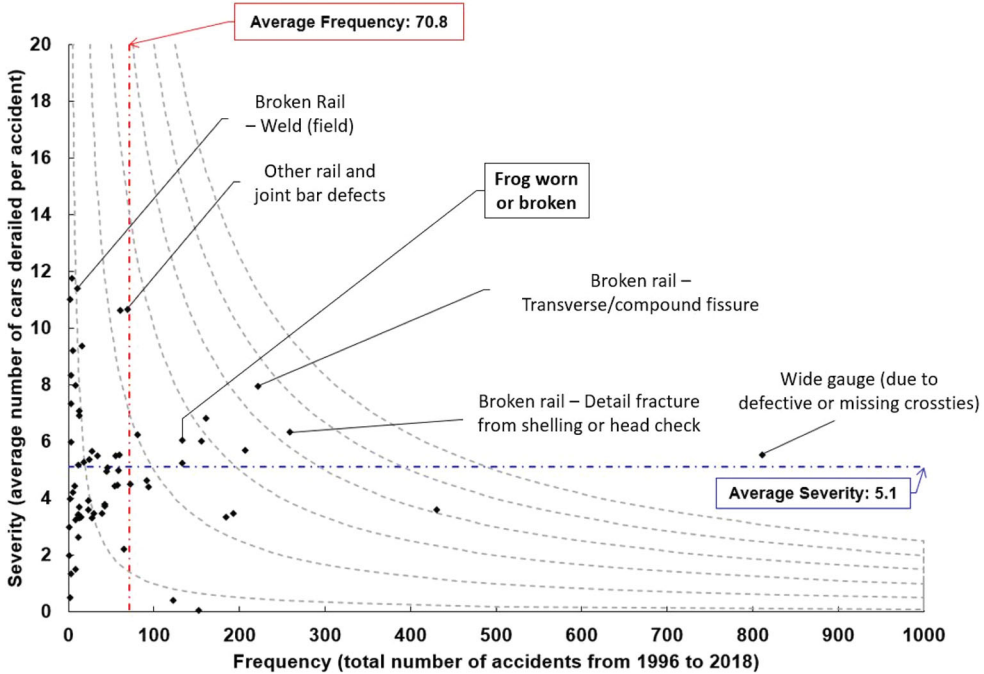


Figure 1. FRA train accident data from 1996 to 2018 depending on frequency and severity [2].

Federal Railroad Administration (FRA) data from 1996 to 2018 on Class I main lines, a total of 119 accidents were caused by a worn and/or broken frog. Furthermore, frog-caused accidents occur with above-average frequency and severity when compared to other track-related derailment causes as shown in Figure 1 [2].

Most turnouts consist of three regions: the switch area which includes the points, the closure area, and the frog area which includes the frog itself and ends at the last long sleeper [3]. Among these, the switch and its associated components and the frog are the most critical turnout components. They require frequent inspection, have maintenance interventions that are disproportionately frequent compared to open track, and result in high life-cycle costs when compared to many other elements of the track structure [4]. Especially, frog generally induces high impact loads as the wheel traverses through the turnout which causes recurring maintenance interventions due to their degradation as a function of tonnage [5]. This can primarily be attributed to the geometry of the rail in the frog that includes a gap (i.e. flangeway) between the wing rail and the point. These impact loads accelerate rail damage in the form of excessive wear, fatigue, plastic deformation, surface cracking and crumbling, shelling and global fracture [6–8].

To improve frog performance and mitigate deterioration, studies have been conducted on wheel–frog interaction. Much of the research has focused on frog geometry optimisation (e.g. modification of frog dimensions, frogs without a discontinuity like spring frogs or movable-point frogs, etc.) and frog material modification. Zboril et al. [9] compared the performance of two different frog materials through field measurements and indicated that hardened surface (340 BHN) frog underwent less material wear after 6.5 MGT (i.e. 0.039 in. (1.0 mm)) than the existing (200 BHN) frog (i.e. 0.094 in. (2.4 mm)). Markine

[10] conducted an experimental study of frogs using 3D acceleration sensors and showed that type of rolling stock and frog geometry have a strong influence on the location of impact contact on the frog and its resulting damage. Li et al. [11] collected field measurements and conducted finite element modelling to analyse the performance of frog sections and concluded that adjusting wheel–rail contact geometry is more effective to improve the performance of turnout frogs compared to changes in rail pad stiffness. Similarly, Grosioni et al. [3] identified the most common turnout frog defects as wear, fatigue and plastic deformation. Furthermore, they report that even though changes in material can be effective in reducing frog damage (e.g. squat failure), optimisation of the frog contact surface and superstructure support stiffness improvement are the most effective methods for improving frog performance [1,12–15].

Given the importance of frog geometry to the improvement of the dynamic interaction between the wheel and frog, this paper presents an investigation of frog profile geometry optimisation based on a set of revenue service wheel profiles. The objective of this research is to reduce frog wear and damage to increase the life cycle and reduce life cycle costs of turnout frogs.

Approach

A review of the literature reveals a variety of studies on frog geometry optimisation. Wan et al. [16] utilised the VI-rail moving track model [17] to consider 25 different frog geometries, and demonstrated frog geometry to have a considerable influence on turnout behaviour by comparing contact point location and maximum contact pressure for each case. Jimenez et al. [18] studied premium frogs by changing the length of the point slope from 10 in. (254 mm) to 15 in. (381 mm), increasing point thickness and employing a conformal frog geometry (i.e. frog with lateral wing rail slope). A performance evaluation was conducted for both standard and premium frogs using visual inspections and quantification of wear and deformation of the running surfaces as a function of time and tonnage. Results show a reduction in deformations of 50% at the point and 33% at the wing for the premium geometry compared to standard. Additionally, given existing frog designs do not accommodate a smooth transition from wing to point for either new or severely hollow worn wheels, Davis et al. [19] manipulated the longitudinal profile for both point and wing. Compared to the conventional frog, the new frog geometry showed less running surface height loss, a 50% reduction in grinding maintenance, and improved dynamic performance as quantified by vertical dynamic loads magnitudes. Nicklisch et al. [12] proposed an optimised transition geometry and support stiffness of the superstructure with the goal of minimising material degradation at wing and point induced by passing wheels. Three frog geometries were introduced and compared in terms of maximum normal contact force and equivalent stress.

Given prior research has identified the importance and influence of frog profile geometry, this study presents a parametric optimisation analysis based on a set of representative revenue service wheel profiles. For the study, a #20 Rail-Bound Manganese (RBM) heavy-point conformal frog was considered as the standard geometry. A total of 30 different frog geometries were derived based on three variables: point slope, relative height difference between wing and point, and longitudinal wing slope. Wheel impact was quantified based on transfer point distribution and vertical wheel trajectory of 400 representative revenue

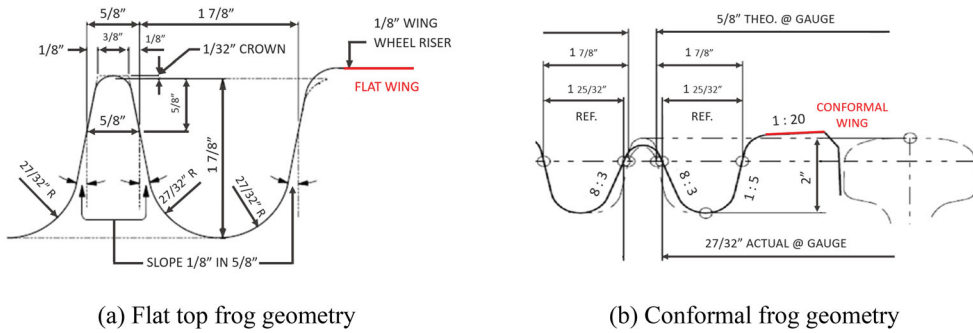


Figure 2. Example geometry of frog designs in N.A. [21]: (a) flat top frog geometry and (b) conformal frog geometry.

service wheel profiles by using a static contact analysis algorithm developed and deployed in Python.

Methodology

Frog geometry

There are a variety of frog geometries and designs used throughout the world including Rail-Bound Welded (RBW), Welded Boltless Manganese (WBM), Welded Spring Manganese (WSM) and RBM. The heavy-point RBM frog design was selected for this study given this design is widely adopted in N.A. due to its rigid structure [20]. Figure 2 presents cross sections of two of the most common RBM frog geometries used in N.A. (i.e. flat top and conformal).

The flat-top frog design obtains its name from the flat running surface of the wing rail (Figure 2a). This flat geometry has been shown to lead to higher contact stresses at the wing corner (i.e. fillet) caused by the mismatch between wing and wheel profiles which can result in higher wear rates and maintenance costs [22]. To address these challenges and improve contact interactions between the wheel and running surface of the wing, the conformal frog geometry was developed by researchers considering the worn profile of the wing on flat-top frogs and the design profile of N.A. wheels [21]. This new design was widely adopted by all Class I railroads starting in the early 2000s and includes a 1:20 lateral wing slope which was designed to match the unworn wheel profile [21]. Additionally, the flat top design employs a heavy-point geometry which consists of a wider point designed to provide additional wear resistance and safety benefits as compared to traditional frog geometry [23]. This heavy point design is the most commonly design used on primary HAL freight mainlines in N.A. The configuration of #20 RBM heavy point conformal frog used in this study is shown in Figure 3. The analysis considered cross sections between 8 and 40 in. from the theoretical point of frog (TPF), the region where the wheel transfer from wing to point generally occurs.

Revenue service wheel profiles

Wheel profile data used in this research were obtained from revenue service Wheel Profile Measurement Systems (WPMs), also known as Wheel Profile Detectors (WPD) (Figure 4)

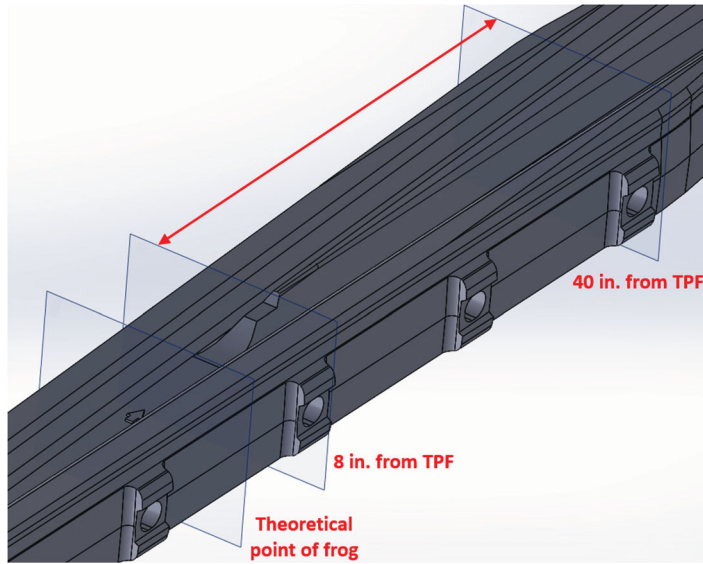


Figure 3. Heavy point conformal frog geometry configuration.

[24]. These wayside detectors capture wheel profile measurements using a laser-based scanning system coupled with high-speed digital cameras. Data output from WPMSs include profile contour as well as calculated parameters such as flange height, flange thickness, rim thickness and hollow tread (HT) which are used to evaluate wheels for interchange compliance, preventative maintenance, maintenance scheduling and derailment prevention purposes. WPMSs have been instrumental over the last decades in removing bad actor wheels from circulation, thus mitigating track and rolling stock damage caused by excessively worn wheels. For the following analysis, a dataset of one million wheel profiles was obtained from a major Class I railroad. The data were captured using four WPMSs from two different vendors, and the WPMS used for the data collection is capable of wheel diameter measurements at high speeds of up to 85 mph (140 km/h), and is operable in temperature ranges from -40°C to 55°C . Three different examples of collected wheel profile data with comparison to AAR-2A standard profile are presented in Figure 4 [25].

Representative wheel subset selection

To reduce the computational demand of this study, a representative subset of wheel profiles was extracted from the larger population. The Slovin formula (Equation 1) was employed to define the minimum number of samples required to adequately represent the population [26].

$$n = \frac{N}{1 + Ne^2} \quad (1)$$

where n is the number of representative samples; N is the total population, and e is the error tolerance related with the confidence level.

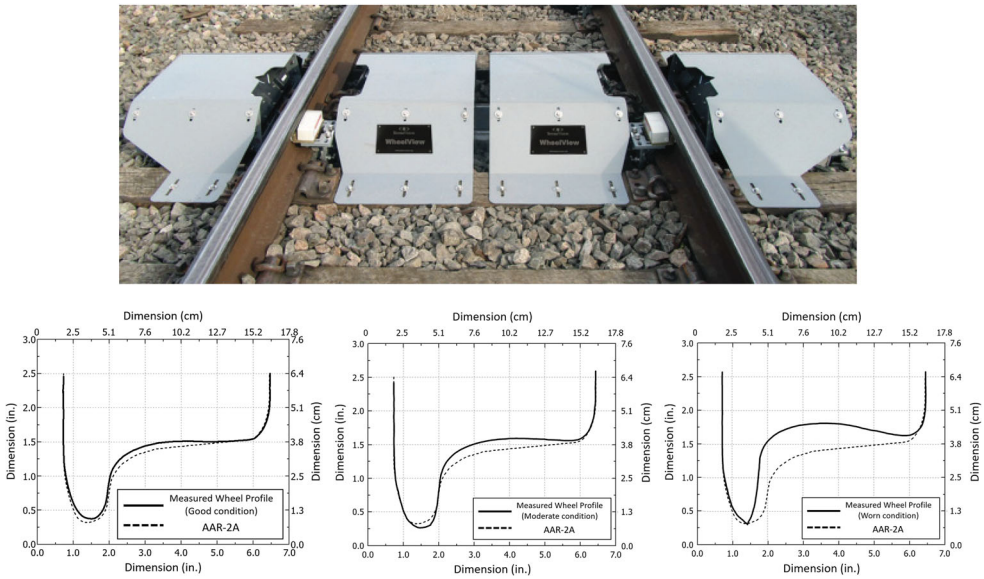


Figure 4. WPMS (top) and wheel profile data example comparison to AAR-2A profile (bottom) [24,25].

Using this methodology, and assuming a reasonable confidence level of 0.05, a 400-wheel sample is needed. However, random sampling of 400 wheels from the population can result in biased conditions of wheels (i.e. dominance of good wheel condition). Therefore, a recent wheel profile classification and stratification methodology developed by Lee et al. [25] for N.A. wheel profiles was employed. Lee et al. defined five different wheel classification types based on tread wear, from wheel Type A (i.e. HT from 0 to 1 mm) through wheel Type E (i.e. HT more than 4 mm) with percentages for each wheel type of 77%, 17%, 4%, 1.5% and 0.3%, respectively. Using this method, the authors randomly extracted 308 Type A, 68 Type B, 17 Type C, 6 Type D and 1 Type E wheels from the population of data, and specific dimensions for each wheel type are described in the previous study [25].

Statistical comparison between sample and population distributions

To further ensure that the selected samples were statistically representative of the population, the distributions of the four-wheel profile geometry parameters (i.e. flange height, flange thickness, hollow tread and rim thickness) were compared between the sample and population.

A normality test was first conducted to determine the methods for comparison of each parameter. A quantile-quantile (Q-Q) plot was selected to test the normality of the distributions as the more commonly used Shapiro–Wilk test is more appropriate for smaller sample sizes (i.e. less than 50) [27,28]. Q-Q plot result (Figure 5) indicates that all the parameters, except for hollow tread, are normally distributed. For the normally distributed parameters (i.e. flange height, flange thickness and rim thickness), an independent sample *t*-test was performed [29]. The non-normal hollow tread distributions were then evaluated using the Kolmogorov–Smirnov (K-S) test [30]. Results from all tests (Table 1)

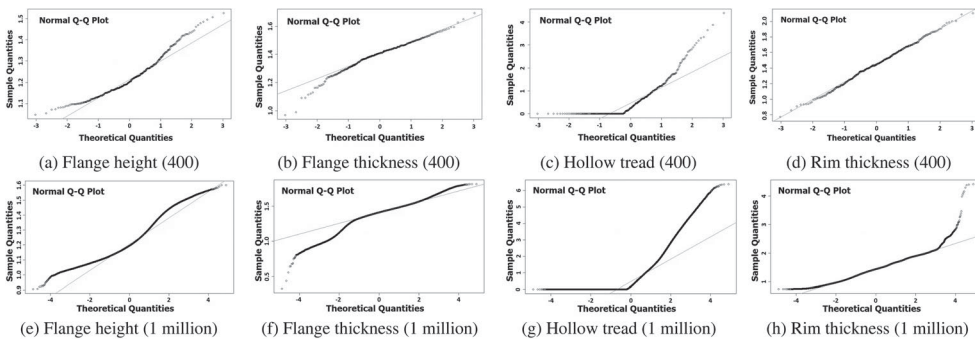


Figure 5. One million and 400 wheel profile Q-Q plot for each four parameters: (a) Flange height (400), (b) Flange thickness (400), (c) Hollow tread (400), (d) Rim thickness (400), (e) Flange height (1 million), (f) Flange thickness (1 million), (g) Hollow tread (1 million), (h) Rim thickness (1 million).

Table 1. *T*-test and *K*-S test *p*-value results for four different wheel parameters.

	Flange height	Flange thickness	Hollow tread	Rim thickness	Note
<i>T</i> -test	0.8700	0.0940	–	0.3243	If $P > 0.05$, two distributions considered same
<i>K</i> -S test	–	–	0.3917	–	

demonstrate that with a significance level of 5% (alpha of 0.05) the two distributions are statistically equal for all four parameters.

Parameter selection

Previous studies have investigated frog geometry optimisation by leveraging parameters such as guard rail/stock rail distance, wing/point distance, and frog point and wing start locations [12,16,18,19]. In this study, two primary frog design elements were considered for optimisation. First, the wheel transfer location should be well distributed throughout the frog length to prevent stress/wear concentration. Second, the transition from wing to point should be smooth with minimised changes in vertical wheel trajectory (i.e. low impact). As a result, three parameters were considered in the subsequent analysis that encompasses the broader design elements introduced earlier: point slope, relative height between wing and point at 26 in. (66 cm) from TPF (i.e. ΔZ_1), and the relative height difference between wing and point at 40 in. (102 cm) from TPF (i.e. ΔZ_2) which generates longitudinal wing slope.

A total of 30 different design cases were considered in this study with three values of point slope, five of ΔZ_1 and two of ΔZ_2 (Figure 6). The specific values for each parameter were selected based on a review of revenue service wheel tread profile data.

First, point slope plays an important role in determining the transfer point location from wing to point. The existing geometry consists of a steep slope from 11.5 in. (29.2 cm) to 16.5 in. (41.9 cm) from the TPF (slope of 1:8) and is flat from 16.5 in. (41.9 cm) onwards, which can lead to wheel transfer concentration at the region with a steep slope. For this reason, and the desire to spread the region of wheel transfer more broadly, two different gradual point slopes (1:36 and 1:65) from 11.5 in. (29.2 cm) to 26 in. (66 cm) were selected as parameters with the same length interval at 11.5 in. (29.2 cm) from TPF.

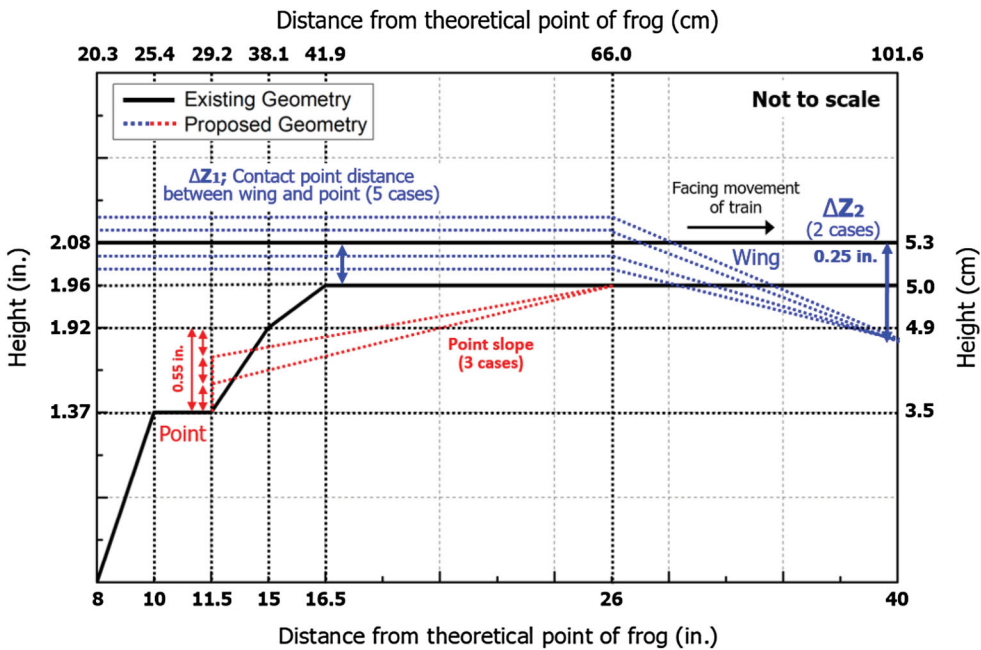


Figure 6. Configuration of different frog geometries evaluated, including existing.

Next, five design cases were selected to evaluate the influence of ΔZ_1 , with dimensions referenced from the existing geometry. These were -0.083 in. (2.1 mm), -0.018 in. (0.46 mm), existing, $+0.017$ in. (0.43 mm), and $+0.041$ in. (1.04 mm) as shown in Figure 6. These parameters were determined using the vertical distance (defined as ΔZ) between the estimated contact points in the wheel tread with the wing and frog point (Figure 7). The ΔZ value depends primarily on the wheel tread profile. For most cases (i.e. new and moderately worn wheels), wing contact location is higher than point contact location and it is defined as a positive ΔZ (Figure 7a and 7b). Conversely, for worn wheels with severe hollow tread wear, the wing contact point can be lower than the frog point contact due to the false flange and its resulting negative ΔZ value (Figure 7c). By design, wheel transfer – between wing and point – will occur at the location along the frog where ΔZ equals the vertical distance between wing and point. Given this, the distribution of ΔZ for the representative sample of wheels investigated in this study was analysed (Figure 8). In addition, the 20th, 40th, 60th and 80th percentiles were selected to complete the five values of ΔZ_1 for the parametric study.

Lastly, the height difference between wing and point at 40 in. (101.6 cm) from the TPF (ΔZ_2) was selected considering the vertical distance required to ensure hollow worn wheels could be transferred from wing to point. Given their negative ΔZ value and the fact that the wing rail is never lower than the point in the existing frog geometry design these wheels would typically only transfer by ‘dropping’ onto the point due to the loss of support from the diverging wing rail. As a starting point, the Association of American Railroads (AAR) interchange limit of 4 mm (0.157 in.) of hollow tread was considered given that only 0.35% of wheels in the population were found to be above this limit [31]. Next, 300 wheels with hollow tread between 3.9 and 4.1 mm (0.154 and 0.161 in.) were randomly

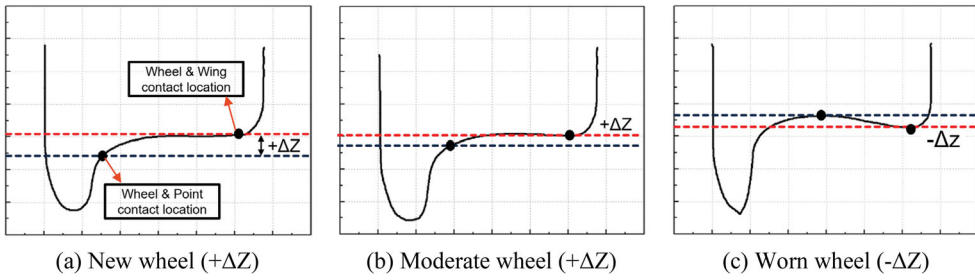


Figure 7. Contact location for different example wheel tread profile conditions identifying the ΔZ value: (a) new wheel ($+\Delta Z$), (b) moderate wheel ($+\Delta Z$) and (c) worn wheel ($-\Delta Z$).

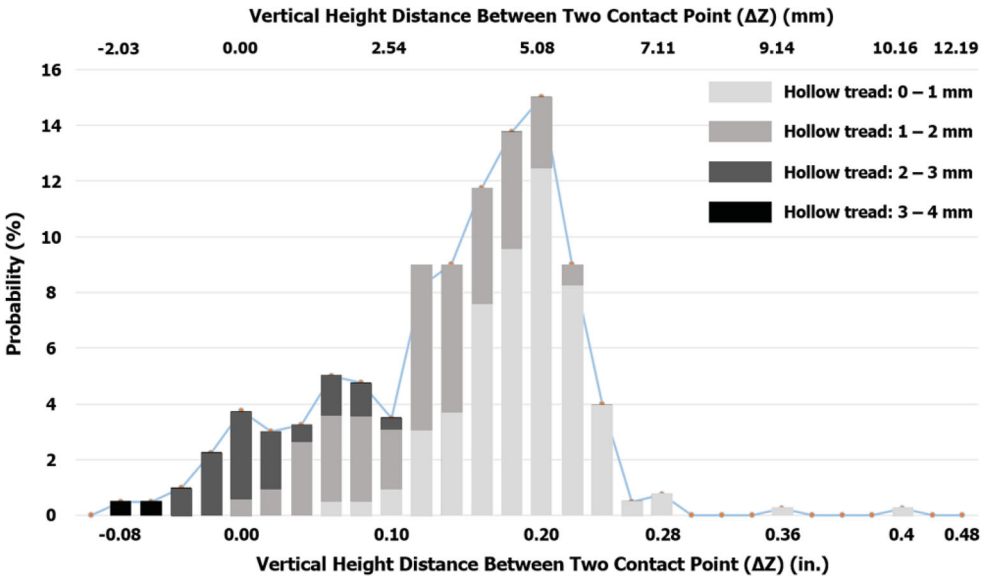


Figure 8. Distribution of ΔZ value for representative 400-wheel sample.

selected from the total population and the respective ΔZ value was calculated for each wheel (Figure 8). Based on the distribution of results obtained, the 75th percentile of ΔZ (i.e. 0.08 in. (2.032 mm)) was selected, and considering this value and the existing difference in elevation between point and wing resulted in the selection of a ΔZ_2 value of 0.25 in. (6.35 mm).

Considering the three parameters described above, a total of 30 unique frog geometry cases were generated and shown below (Table 2). Frog geometry characteristics that were not specifically mentioned above were held constant at the value of the existing conformal heavy point frog geometry (Figure 6).

Analysis procedure

The analysis was conducted using algorithms developed and implemented in Python. The baseline frog geometry was established using a Solidworks model and first extracted to

Table 2. 30 different frog geometry cases.

Item	Case #1	Case #2	Case #3	Case #4	Case #5	Case #6	Case #7	Case #8	Case #9	Case #10
Point slope	1:36									
ΔZ_1 in. (mm)	-0.083 (-2.11)	-0.018 (-0.46)	Existing	0.017 (0.43)	0.041 (1.04)	-0.083 (-2.11)	-0.018 (-0.46)	Existing	0.017 (0.43)	0.041 (1.04)
ΔZ_2 in. (mm)	-	-	-	-	-	-0.25 (-6.35)	-0.25 (-6.35)	-0.25 (-6.35)	-0.25 (-6.35)	-0.25 (-6.35)
Item	Case #11	Case #12	Case #13	Case #14	Case #15	Case #16	Case #17	Case #18	Case #19	Case #20
Point slope	1:65									
ΔZ_1 in. (mm)	-0.083 (-2.11)	-0.018 (-0.46)	Existing	0.017 (0.43)	0.041 (1.04)	-0.083 (-2.11)	-0.018 (-0.46)	Existing	0.017 (0.43)	0.041 (1.04)
ΔZ_2 in. (mm)	-	-	-	-	-	-0.25 (-6.35)	-0.25 (-6.35)	-0.25 (-6.35)	-0.25 (-6.35)	-0.25 (-6.35)
Case #23										
Item	Case #21	Case #22	(Existing)	Case #24	Case #25	Case #26	Case #27	Case #28	Case #29	Case #30
Point slope	Existing point slope									
ΔZ_1 in. (mm)	-0.083 (-2.11)	-0.018 (-0.46)	Existing	0.017 (0.43)	0.041 (1.04)	-0.083 (-2.11)	-0.018 (-0.46)	Existing	0.017 (0.43)	0.041 (1.04)
ΔZ_2 in. (mm)	-	-	-	-	-	-0.25 (-6.35)	-0.25 (-6.35)	-0.25 (-6.35)	-0.25 (-6.35)	-0.25 (-6.35)

CAD and then to Excel. 30 different frog geometries were created by modifying the existing geometry as shown in Table 2. The contact analysis procedure followed the following steps: (1) position wheel at 8 in. (20.3 cm) from TPF longitudinal direction and at 4 in. (10.2 cm) above wing rail, (2) lower wheel in 0.05 in. (1.3 mm) increments until both profiles (i.e. wheel and wing) overlap, (3) move wheel profile 0.1 in. (2.5 mm) toward point and (4) repeat steps 2–3 until wheel contacts opposite wing rail. These steps will be repeated for each frog cross section (0.5 in. increment) from 8 to 40 in. (20.32 cm to 101.6 cm) from the TPF. An assumption was made that the back-to-back distance of all wheels is consistent, and the lateral wheel movement was restricted based on standard guard rail clearances.

Impact quantification

Wheel–rail interaction is dependent on a variety of factors, including wheel–rail contact, train speeds, mechanical properties of train and track, and track geometry. In the frog area, the wheel's vertical trajectory is not smooth and is known to present a dip-like shape (Figure 9). Several studies have quantified the impact generated by wheels passing through frogs [32–35]. Within these, Pletz [32] described a simplified method to estimate the impact on the frog from the vertical wheel trajectory while traversing the turnout as illustrated in Figure 9.

Based on this methodology, the impact can be estimated by considering the train speed (v), impact angle (α) and mass of the wheel (m_{wheel}) as is shown in Equation (2):

$$P = v \times \alpha \times m_{wheel} \quad (2)$$

In this study, the wheel mass and speed of train are assumed to be constant for all cases, thus only the impact angle (α) was used to calculate impact (P) for each frog design case.

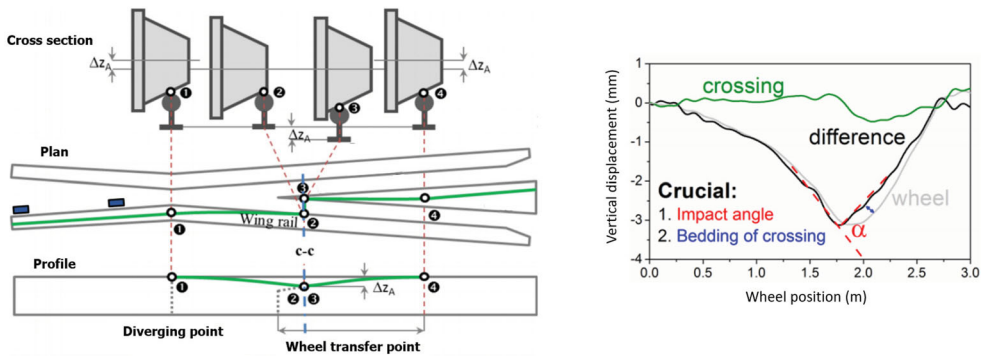


Figure 9. Vertical wheel trajectory in turnout transition zone demonstrating the impact angle (α) [32,33].

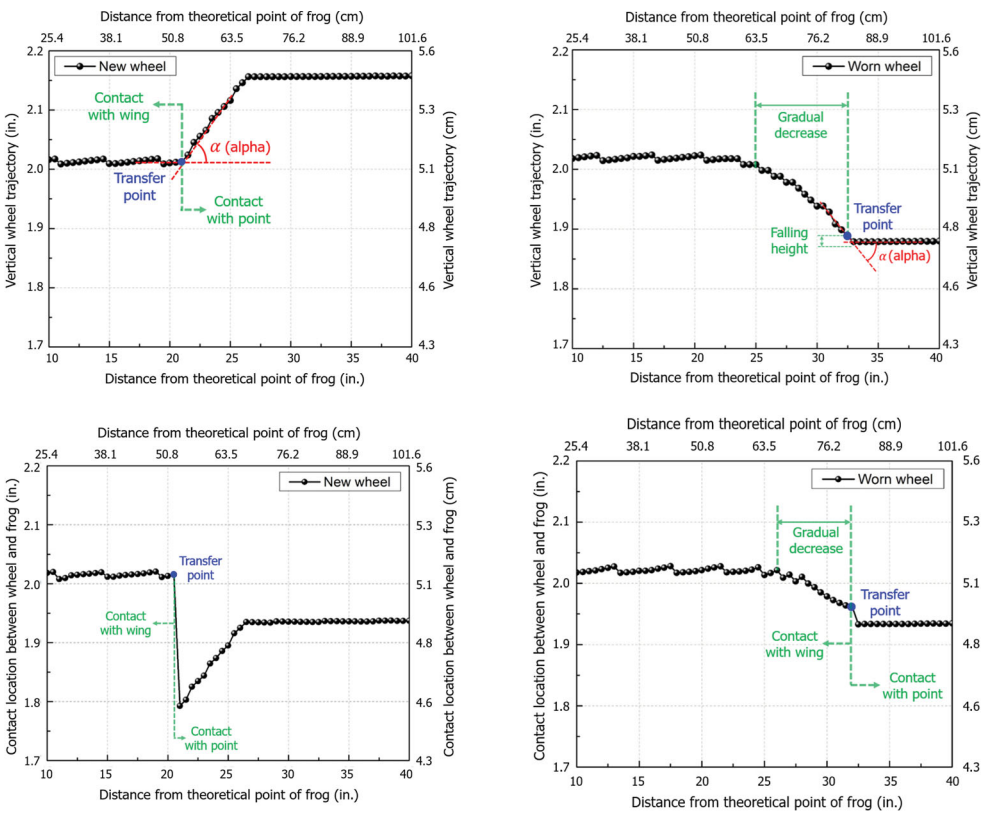


Figure 10. Vertical wheel trajectory (top) and contact location (bottom) for new and worn wheel.

New and worn wheel examples are shown in Figure 7, and the vertical wheel trajectory and contact point location between wheel and frog (Case #1) for both new and worn wheel are shown in Figure 10.

New wheels were shown to have stable vertical wheel trajectory before the transfer point while a worn wheel presents a gradual decrease of vertical trajectory (lateral direction

wheel movement) as it approaches the transfer point (Figure 10, top). These differ from the behaviour demonstrated in Figure 9 and are due to the conformal geometry of the wing in the frog under study. Specifically, for the flat top geometry (Figure 2a and Figure 9), the flat wing results in a downward trajectory of the wheel before the transfer as the wing support moves outwards on the conical wheel tread. Conversely, in the conformal geometry, the lateral slope of the wing compensates for the wheel tread shape and allows the wheel to maintain its vertical trajectory. This lowers the impact angle (α) compared to flat top geometry which aligns with the purpose of conformal frog geometry. After the transfer point, upward movement was observed in the new wheel as it climbs the point slope while the worn wheel falls on to the point once the wheel loses support from the wing rail. Based on the vertical wheel trajectory, the impact angle α can be calculated for each combination of wheel and frog geometry as shown in Figure 10 (top).

Contact location results presented in Figure 10 (bottom) demonstrate both new and worn wheels only contact the wing rail before the transfer occurs. After transfer, the new wheel showed substantial lateral shift in contact position, which demonstrates the contact point of the frog was changed from wing to point. For the worn wheel, the lateral shift in contact position was observed after gradual decrease behaviour (same with vertical wheel trajectory result).

Based on the behaviour observed above, the amount of impact for each section of frog was calculated for all 400 wheels and 30 different geometries using the impact angle α , and total impact was derived for each case by adding all impacts for every section.

Analysis results

Individual effects of each parameter

Transfer point analyses were performed using the values selected for the three critical geometry parameters that were previously introduced (i.e. point slope, ΔZ_1 , and ΔZ_2). Transfer point distributions were generated (Figure 11) by varying each parameter while holding all other dimensions constant at their baseline design values. This allowed examination of the individual effect of each parameter on the transfer distribution performance of different designs.

Results demonstrate that the three different point slopes show considerable differences in transfer location from 10 in. (25.4 cm) to 27 in. (68.6 cm). For Case #13 (i.e. 1:65 slope), around 15% of wheel transfers are observed at 11.5 in. (29.2 cm) due to the higher height of the point tip with a gradual point slope compared to other cases. Comparatively, Case #3 (i.e. 1:36 slope) showed no transfers at this location leading to higher number of transfers between 22.5 in. (57.2 cm) and 26.5 in. (67.3 cm). Lastly, the existing geometry showed higher transfer of wheels from 11.5 in. (29.2 cm) to 16.5 in. (41.9 cm), where the point slope exists, after which most wheels that were not picked up by the point slope were then transferred late into the frog, between 27 in. (68.6 cm) and 38 in. (96.5 cm).

Next, the effect of ΔZ_1 was evaluated and showed considerable differences between 11.5 in. (29.2 cm) to 16.5 in. (41.9 cm). For Case #21 (i.e. ΔZ_1 of -0.083 in.), more than 40% of wheels transfer at 11.5 in. (29.2 cm) due to the low wing height. By increasing the ΔZ_1 value from Case #21 to Case #25, the number of wheels transferred around 11.5 in. (29.2 cm) decreases greatly.

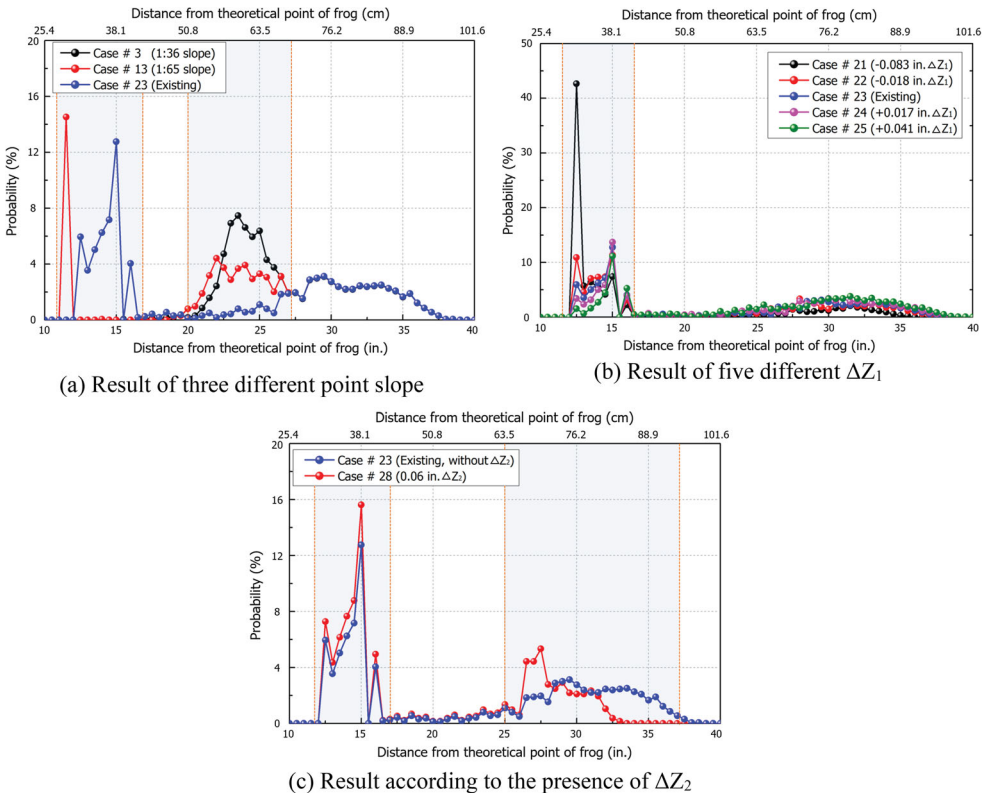


Figure 11. Transfer point distribution analysis results depending on each parameter: (a) result of three different point slope, (b) result of five different ΔZ_1 , (c) result according to the presence of ΔZ_2 .

Lastly, the effects of the introduction of a longitudinal wing slope (i.e. ΔZ_2) to the frog design were evaluated. Similar result of transfer distribution was observed except for the section from 26 in. (66 cm) to 40 in. (101.6 cm). For the design with ΔZ_2 (i.e. Case #28), the majority of wheels (including hollow worn wheels) are transferred before 32 in. (81.3 cm) due to the presence of the longitudinal wing slope that lowers wheels onto the point. However, results for the existing geometry (without ΔZ_2) showed the last wheel transfer at 38 in. (96.5 cm), with such transfers being hollow worn wheels.

Based on the results observed, different parameters affect the wheel-frog interaction at different locations and an optimised frog geometry needs to ensure a well-distributed wheel transfer location to avoid transfer concentration which may lead to high degradation, and low total impact (i.e. low α) at the transfer point from wheel to point. Therefore, by combining the appropriate dimension for each parameter, and based on the total impact for each case, an optimised frog geometry case is proposed in the following section.

Impact comparison

The total impact from wheel to frog was quantified using Equation (2) and considering the vertical wheel trajectory for each geometry case. Results obtained were normalised to the

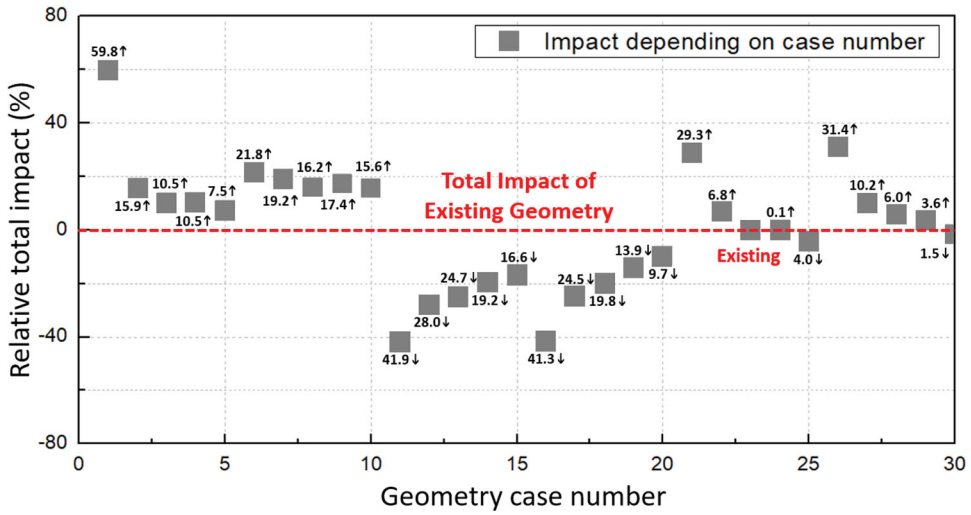


Figure 12. Quantified relative total impact for all frog geometry cases.

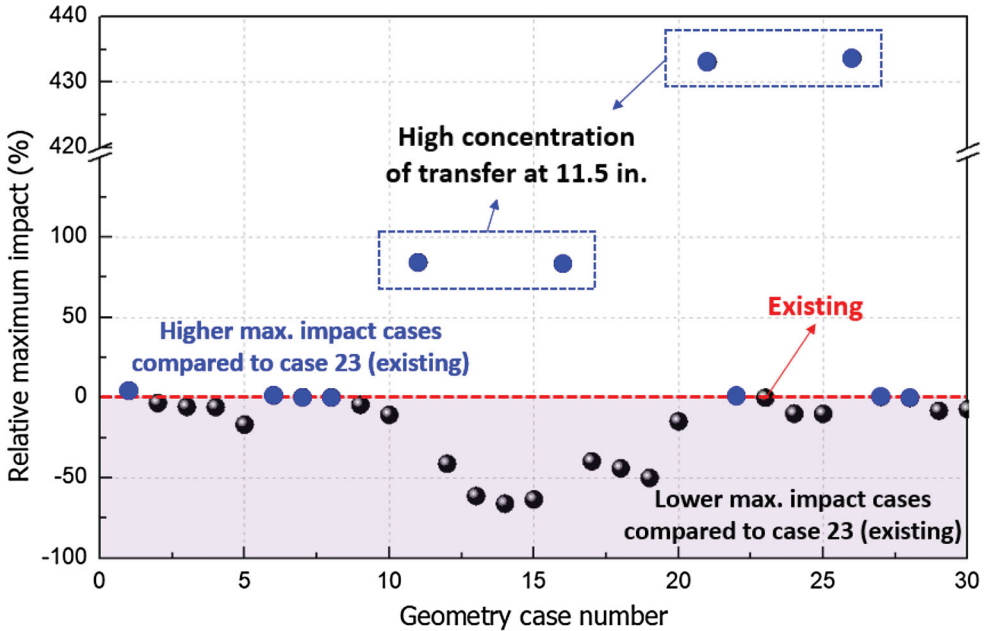


Figure 13. Quantified relative maximum impact for each frog geometry case.

total impact results of the existing geometry case and the relative total impact for each case is presented in Figure 12.

Additionally, to avoid wheel transfer concentration, the maximum impact quantified at a specific section for each geometry case results are shown in Figure 13.

Compared to the existing geometry (i.e. Case #23), Cases #1 to #10 (1:36 point slope) showed higher total impacts while Cases #11 to #20 (1:65 point slope) showed lower total impacts. This finding demonstrates that total impact is more greatly affected by differences

in point slope as compared to the other two parameters. In evaluating an optimised frog geometry, Case #11 showed the lowest total impact with a 42% decrease compared to the existing geometry case. However, as previously mentioned, it is also important to avoid high concentrations of transfers which may lead to high degradation. In this regard, Cases #1, #6, #7, #8, #11, #16, #21, #22, #26, #27 and #28 were excluded as optimal geometries as they presented higher impact at specific section than the existing geometry (Figure 12). Therefore, the remaining 19 cases, including the existing frog geometry, were compared using the total impact, and Case #12 (point slope of 1:65, ΔZ_1 of -0.018 in. and without wing slope (ΔZ_2)) showed the greatest relative impact reduction of -28% compared to the existing geometry (Case #23).

Conclusion

This paper presented a parametric study to optimise the geometry of a railway turnout frog by lowering the total impact from wheel to frog and avoiding impact concentration based on result of transfer point distribution and vertical wheel trajectory from a static profile interaction model. Three parameters (i.e. point slope, ΔZ_1 and ΔZ_2) were considered and their effects were investigated and quantified. From the evaluation of the impact results for 30 different frog geometry cases using 400 representative wheel profiles, the following conclusions are presented:

- Transfer point distribution analysis result indicated that each parameter affects different locations of frog geometry and proper combination of these is essential to reach an optimised geometry. Mainly affected regions are: 10 in. (25.4 cm) to 27 in. (68.6 cm) for point slope; 26 in. (66 cm) to 40 in. (101.6 cm) for ΔZ_1 and 26 in. (66 cm) to 38 in. (96.5 cm) for ΔZ_2 .
- To estimate the impact from wheel to frog, impact angle α (i.e. dip angle of wheel vertical trajectory) was calculated for each wheel and geometry case. Based on the methodology applied in this study, total impact was more significantly affected by frog geometry than by wheel condition.
- Based on the calculated α values and transfer point distribution, total impact for each 30 geometry cases was derived and compared. Although Case #11 showed largest total impact reduction (i.e. -41%) it was excluded due to high concentration of impacts at a single point (i.e. 11.5 in. (29.2 cm)). Therefore, Case #12 (point slope of 1:65, ΔZ_1 of -0.018 in. (-0.46 mm) and without wing slope (ΔZ_2)) with -28% reduction in total impact was selected as the most optimised frog geometry for this study.
- Although the existence of ΔZ_2 (which creates a longitudinal wing slope) can avoid late transfers from wing to point, the methodology used in this paper showed minimal impacts from late-transfer wheels.

The above conclusions provide an estimate of the response of the wheel–frog interaction with the changes in dimensions for three frog geometry parameters. Furthermore, by conducting this parametric study, an optimised frog geometry with reduced impact was proposed. However, it should be noted that the analysis method employed in this study is solely based on static geometric interaction and does not reflect all possible dynamic interaction and impact conditions. Therefore, dynamic and contact modelling should be

performed in subsequent studies to further understand the dynamic interactions with field measurement used for model validation.

Acknowledgements

The authors would like to thank graduate research assistants Ryan Harrington and Ian Germoglio Barbosa for assisting in finding and organising many of the reference sources. J. Riley Edwards was supported in part by grants to the University of Illinois' Rail Transportation and Engineering Center (RailTEC) from CN and Hanson Professional Services.

Disclosure statement

No potential conflict of interest was reported by the author(s).

Author contribution statement

The authors confirm contribution to the paper as follows: study conception and design: J. Lee, A. de O. Lima, J. R. Edwards, and M. S. Dersch; data collection: J. Lee, A. de O. Lima, J. R. Edwards, and M. S. Dersch; analysis and interpretation of results: J. Lee, A. de O. Lima, J. R. Edwards, and M. S. Dersch; draft manuscript preparation: J. Lee, A. de O. Lima, J. R. Edwards and M. S. Dersch. All authors reviewed the results and approved the final version of the manuscript.

ORCID

Jaeik Lee  <http://orcid.org/0000-0003-3990-9820>

Arthur de O. Lima  <http://orcid.org/0000-0002-9642-2931>

Marcus S. Dersch  <http://orcid.org/0000-0001-9262-3480>

J. Riley Edwards  <http://orcid.org/0000-0001-7112-0956>

References

- [1] Pålsson BA. Optimisation of railway crossing geometry considering a representative set of wheel profiles. *Veh Syst Dyn.* 2015;53(2):274–301. DOI:10.1080/00423114.2014.998242.
- [2] Federal Railroad Administration Office of Safety Analysis: Accident Data as reported by Railroads. [cited 2022 June 10] Available from: https://safetydata.fra.dot.gov/OfficeofSafety/publicsite/on_the_fly_download.aspx.
- [3] Grossoni I, Hughes P, Bezin Y, et al. Observed failures at railway turnouts: failure analysis, possible causes and links to current and future research. *Eng Fail Anal.* 2021;119. DOI:10.1016/j.engfailanal.2020.
- [4] Zwanenburg WJ. A model for the life expectancy of railway switches and crossings for maintenance and renewal planning in asset management systems. *Comp Railw XI.* 2008;I:765–773. DOI:10.2495/CR080741.
- [5] Skrypnyk R, Nielsen JCO, Ekh M, et al. Metamodelling of wheel–rail normal contact in railway crossings with elasto-plastic material behaviour. *Eng with Comp.* 2019;35:139–155. DOI:10.1007/s00366-018-0589-3.
- [6] Dahlberg T. State-of-the art study on railway turnouts: dynamics and damage. Chalmers: Tekniska Högskola; 2004.
- [7] Wan C, Markine VL, Shevtsov IY, et al. Improvement of train-track interaction in turnouts by optimising the shape of crossing nose. Proceedings of the 23rd inter symp on Dyn of Veh on roads and tracks (IAVSD); 2013 Aug 19–23; Qingdao, People's Republic of China.
- [8] Nissen A. Development of life cycle cost model and analyses for railway switches and crossings [dissertation], Luleå: Luleå University of Technology; 2009.

- [9] Zboril J, Havlicek P. Wear of the railway turnout crossings made of explosive hardened Hadfield steel. *Metal* 2013; 2013 May 15–17; Brno, Česko.
- [10] Markine VL. An experimental study on crossing nose damage of railway turnouts in The Netherlands. The Fourteenth International Conference on Civil, Struc and Environmental Engineering (ICCSEE); 2013 Sep 3–6; Cagliari, Italy.
- [11] Li X. Wheel–Rail impact loads and track settlement in railway crossings [dissertation]. Chalmers: Chalmers University of Technology; 2019.
- [12] Nicklisch D, Kassa E, Nielsen J, et al. Geometry and stiffness optimization for switches and crossings, and simulation of material degradation. *Proc IMechE Part F J Rail Rapid Transit*. 2010;224(4):279–292. DOI:10.1243/09544097JRR348.
- [13] Grossoni I, Bezin Y, Neves S. Optimisation of support stiffness at railway crossings. *Veh Syst Dyn*. 2018;56(7):1072–1096. DOI:10.1080/00423114.2017.1404617.
- [14] Wan C, Markine V, Shevtsov I. Optimisation of the elastic track properties of turnout crossings. *Proc Insti Mech Eng F J Rail Rapid Transit*. 2016;230(2):360–373. DOI:10.1177/0954409714542478.
- [15] Pålsson BA, Nielsen JCO. Dynamic vehicle–track interaction in switches and crossings and the influence of rail pad stiffness – field measurements and validation of a simulation model. *Veh Syst Dyn*. 2015;53(6):734–755. DOI:10.1080/00423114.2015.1012213.
- [16] Wan C, Markine VL, Shevtsov IY. Improvement of vehicle–turnout interaction by optimising the shape of crossing nose. *Veh Syst Dyn*. 2014;52(11):1517–1540. DOI:10.1080/00423114.2014.944870.
- [17] Railway Simulation Software VI-Rail. [cited 2022 June 18]. Available from: <https://simteqengineering.co.za/products/vi-rail/>.
- [18] Jimenez R, Davis D, Shu X, et al. Performance of No. 20 frogs of various designs in revenue service. Pueblo (CO): Transportation Technology Center Inc; 2017.
- [19] Davis D, Singh SP, Guillen DG, et al. Field evaluation of improved performance frog profile designs for heavy axle load service. Pueblo (CO): Transportation Technology Center Inc; 2003.
- [20] Davis D, Chen YR, Lawrence FV, et al. Frog design review and failure analysis. Pueblo (CO): Transportation Technology Center Inc; 2001.
- [21] Voelkerding D. Computer modeling for Low impact frog design. In: Wheel rail interaction (WRI). Nevada: Henderson; 2016 May 2–5.
- [22] Austin M. Conformal frog evolution at CSX. In: American Railway Eng and maintenance-of-Way asso (AREMA). Orlando (FL); 2016 Aug 28–31.
- [23] Rakoczy A, Shu X, Davis D, et al. Heavy point frog FRA report heavy point frog performance under passenger vehicles. Washington (DC): Federal Railroad Administration; 2016.
- [24] Beena vision solutions, automatic In-track wheel profile measurement system. GA. USA. [cited 21 February 2023]. Available from: <https://railway-news.com/wp-content/uploads/2017/01/WheelView-Q4-2014-LowRes.pdf>.
- [25] Lee JI, Dersch MS, Lima ADO, et al. Probabilistic review of wheel profiles based on low tread in the U.S. heavy haul rail network. *Proc IMechE Part F J Rail and Rapid Transit*. 2023;237(4):508–516. DOI:10.1177/09544097221122030.
- [26] Abdullah NAR, Yusriadi J, Yusuf OYH, et al. Analysis of household economic conditions and community habits on The incidence of anemia in pregnant women through household nutrition management in The working area of The salugatta health center, central mamuju regency. International Conference on Indus Engineering and Operations Management (IEOM); 2021 April 5–8. Sao Paulo, Brazil.
- [27] Mishra P, Pandey CM, Singh U, et al. Descriptive statistics and normality tests for statistical data. *Ann Card Anaesth*. 2019;22(1):67–72. DOI:10.4103/aca.ACA_157_18.
- [28] Ghasemi A, Zahediasl S. Normality tests for statistical analysis: A guide for Non-statisticians. *Int J Endocrin Metabol*. 2012;10(2):486–489. DOI:10.5812/ijem.3505.
- [29] Gerald B. A brief review of independent, dependent and One sample t-test. *Int J Appl Mathemat Theort Phy*. 2018;4(2):50–54. DOI:10.11648/j.ijamtp.20180402.13.
- [30] Magel RC, Wibowo SH. Comparing the powers of the Wald–Wolfowitz and Kolmogorov–Smirnov tests. *Biom J*. 1997;39(6):665–675. DOI:10.1002/bimj.4710390605.

- [31] Field manual of the AAR interchange rules. Washington (DC): Association of American Railroads; 2017.
- [32] Pletz M. Damage in railway crossings-numerical models [dissertation]. Leoben: University of Leoben; 2012.
- [33] Sysyn M, Gerber U, Nabochenko O, et al. Indicators for common crossing structural health monitoring with track-side inertial measurements. *Acta Polytech.* 2019;59(2):170–181. DOI:[10.14311/AP.2019.59.0170](https://doi.org/10.14311/AP.2019.59.0170).
- [34] Wiest M, Daves W, Fischer FD, et al. Deformation and damage of a crossing nose due to wheel passages. *Wear.* 2008;265:1431–1438. DOI:[10.1016/j.wear.2008.01.033](https://doi.org/10.1016/j.wear.2008.01.033).
- [35] Bruni S, Anastasopoulos I, Alfi S, et al. Effects of train impacts on urban turnouts: modelling and validation through measurements. *J Soun Vib.* 2009;324:669–689. DOI:[10.1016/j.jsv.2009.02.016](https://doi.org/10.1016/j.jsv.2009.02.016).